euspen's 23rd International Conference & Exhibition, Copenhagen, DK, June 2023

www.euspen.eu

Development of an angular position detection method to accurately characterize high speed spindles without encoders

Tobias Mayer[1], Andreas Lange[1], Alexander Schulz[1], Benjamin Kirsch[1], Jan C. Aurich[1]

[1]*RPTU in Kaiserslautern; Institute for Manufacturing Technology and Production Systems*

tobias.mayer@mv.uni-kl.de

Micro manufacturing processes such as micro milling are widely utilized in in many fields, e.g. bioengineering or microelectronics. Due to the small tool diameters, the spindles used must deliver high speeds to achieve the required cutting speeds. In addition, their runout needs to be low even at those high speeds to avoid increased wear of the filigree tools, and deviations on the workpiece. Therefore, it is necessary to characterize the spindle, so that the runout of the spindle over the entire speed range is known and frequencies with low runout values can be chosen. However, many commercial high speed spindles do not feature rotary encoders, which are necessary to relate the measured runout to the angular position of the spindle shaft. The once per revolution out of roundness error of the clamping system is not precise enough to reliably get the angular information. Measurements over multiple revolutions, or the use of error separation techniques to separate the artifact from the measured data are not possible.

Thus, in this study, we developed an angular position detection using a modified measurement artifact and an additional sensor. Various artifact designs and variants were manufactured, tested, and evaluated. With the final geometry, a peak detection was implemented in the measuring script, and the data points from the other sensors remapped to their angular positions. We showed that with our approach, the errors associated with the simple once per revolution out of roundness method were eliminated. Precise characterization with correct angular information is thus possible, as well as more advanced error separation techniques.

spindle characterization, high speed spindles, capacitive sensors, measurement data analytics, micro milling

1. Introduction

Micro components and micro parts with e.g. functionalized surfaces have become common occurrence in medical devices or consumer goods (such as optics in smart devices) [1]. As a result, the field of micro machining has been extensively researched [2], with micro milling as one of the most prominent processes [3]. Due to the small diameters of the tools, ultra-high speed spindles are required to reach acceptable cutting speeds, while at the same time requiring very low runout [4]. To achieve the best possible results, knowledge of the speed dependent dynamic behavior of the spindle, i.e. the synchronous error motion and its frequency components, are required [5]. However, many commercially available ultra-high speed spindles do not feature rotary encoders, which are usually used to relate the measured sensor data to the angular position of the spindle [6]. This means that the roundness errors measured cannot be separated into errors caused by the spindle and the artifact itself, as these critically depend on the angular position of the spindle [7]. In addition, this introduces errors in the measurement analysis due to error propagation.

As the first data point per revolution is not triggered at the zero-mark of an encoder signal, it is assigned as the first data point recorded for the first revolution. In subsequent revolutions, the position of the data point in the measurement array determines its angular position via the amount of data points acquired per revolution. However, a slight timing offset between the actual zero angular position and the first data point in the following revolutions exists because the spindle and DAQ frequency are not synchronized. As a result, the assumed angular positions are offset from the actual ones, increasing with each revolution measured.

In addition, slight deviations of the spindle frequency can occur, e.g. due to the torque characteristics of the motor. As such, one revolution may contain less or more data points than average. This increases the error offset of the data points, as the angular position information relies on a constant amount of data points per revolution. Figure 1 showcases the effect: One revolution with a higher amount of data points transfers over to all other revolutions afterwards, and the resulting errors in the assumed angular positions become larger.

Figure 1: Error propagation due to changing number of data points per revolution without angular position information: Vector of raw data (a)) and corresponding aligned data matrix (b)).

The behavior shown here results in errors large enough that only few (10 - 20) revolutions can be analyzed to characterize the spindle. Otherwise, the incorrect angular positions result in significant errors, especially when calculating the synchronous error motion: Due to the varying offset of the angular positions, it is seen as a circle regardless of the spindles error motions.

To alleviate this, we developed a method to map the measured data to the actual angular spindle position, which can eliminate the errors detailed above. This allows for calculations of the error motions and enables error separation techniques to be used. We used an additional sensor and modified artifacts to provide a zero-mark more accurate than the once per revolution out of roundness error. Three different artifact geometries were explored, and several geometric parameters tested. We further

implemented a method to accurately find and relate the zero-mark to the spindle position. Finally, we compared the measurements with the data points aligned to the zero-mark versus the ones without alignment.

2. Experimental spindle characterization setup

The high-speed spindle used in the measurements of this study was an aerostatic ABL[1] type MM125 spindle. The spindle features a pneumatically actuated Ø 3 mm collet, a speed range of 15.000 min^{-1} – 125.000 min^{-1}, and a dynamic runout below 3 µm as per manufacturer specification. The spindle is mounted in a three axes desktop machine tool developed at our institute, see [8] for further information. For the spindle characterization, a setup with two capacitive sensors was used. Figure 2 showcases the measurement chain, which consists of the sensor-driver unit for displacement measurement and signal conditioning, a DAQ for sampling, and a laptop for data recording and analysis. The sensors are two Lion Precision[1] model C8-2.0, in combination with CPL190 Elite Series drivers. The sensor range is 250 µm with a resolution of 5 nm @ 15 kHz bandwidth, and a sensitivity of 80 mV/µm. The DAQ used for sampling is a National Instruments[1] USB-6251 with 16bit resolution. In our experiments, each channel was sampled at 250 kHz. Different voltage ranges can be utilized to achieve maximum sensor resolution after the sensor has been aligned with the artifact. Post processing is done in Mathworks[1] MATLAB, filtering the measurement data and computing Fourier transformations, asynchronous and synchronous error motion, and total indicated runout. The script was modified as described in section 4 to allow for the angular position correction, reducing error propagation in the runout calculations.

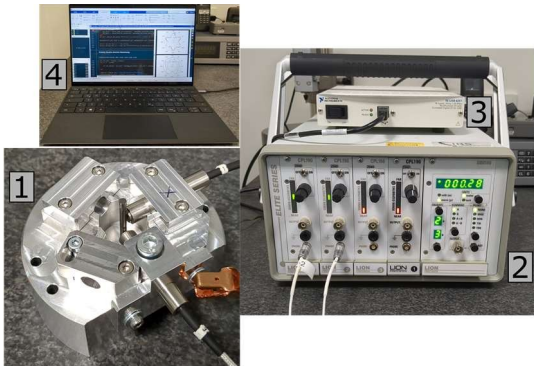

Figure 2: Measurement chain for the spindle characterization hardware used: Sensor holder with capacitive sensors (1), driver electronics (2), DAQ (3) and laptop (4).

The measurement artifacts used were cemented carbide blanks with dimensions Ø 3 mm h6 x39 mm, supplied by Hyperion[1] (manufacturer code PN90, WC/Co, 9% Co).

The approach to eliminate the error propagation detailed in the introductory section was to create a clearly identifiable, once per revolution peak by modifying the measurement artifact geometry and employing an additional sensor to only measure against this modified geometry. The modification is done at the tip of the artifact, so that only the additional sensor used for the angular detection 'sees' it: The sensors used for the measurement are mounted in a plane above the modified artifact surface. They can be used to measure versus the artifact surface as normal, while the additional sensor is installed at the height of the altered geometry. The geometry should be altered in a way that the resulting peak in the sensor signal is maximally sharp. Then it can be discerned from any error motion of the spindle or the clamping system. With that information the angular position of the signal can be inferred, and the data from the measurement sensors referenced to it.

For the sensor to see a change in signal, the artifact geometry needs to be changed by either removing or adding material, or by locally changing the relative permeability. Changing the relative permeability and adding material to the artifact are impractical and difficult to achieve. Removing material from the artifact on the other hand can easily be done using tool grinding machines. We manufactured three different styles of artifacts using two grinding machines (Walter[1] Helitronic Vision for large material removal, and a custom micro tool grinding machine [9] for the single cut-outs).

Figure 3 depicts the geometry of the modified artifacts: The first style (3 a)) features a single cut-out on the surface, where a small amount of material has been removed with a grinding wheel. The second style (3 b)) is a flat ground bar shape for which a large amount of material has been ground away from both sides, only leaving a bar shaped rectangle in the centre of the artifact. The third geometry (3 c)) is a triangular pattern. Similar to the bar shaped artifact, material was removed from three sides to form an equilateral triangle.

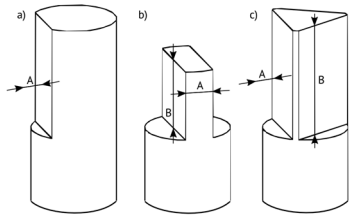

Figure 3: Modified measurement artifacts to detect the angular spindle position: a) cut-out, b) bar shape, c) triangular pattern.

For each artifact variant, the depth of the cut-out or the width of the ground geometry was varied, respectively. For the bar shaped and triangular artifacts the height was varied as well, as a large amount of material had to be removed. Table 1, 2, and 3 show the parameters of the individual variants and their naming.

Table 1: Parameters and naming for the cut-out artifact variants.

C1	C2	C3	C4
A = 38 µm	A = 27 µm	A = 13 µm	A = 9 µm

Table 2: Parameters and naming for the bar shaped artifact variants.

B1	B2	B3	B4
A = 1 mm B = 5 mm	A = 1 mm B = 2.5 mm	A = 0.5 mm B = 5 mm	A = 0.5 mm B = 2.5 mm

Table 3: Parameters and naming for the triangular artifact variants.

T1	T2	T3	T4
A = 0.66 mm B = 8 mm	A = 0.66 mm B = 4 mm	A = 0.58 mm B = 8 mm	A = 0.58 mm B = 4 mm

3. Measurement results for the different artifacts

In the first test series, all artifacts were measured at a typical spindle speed of 30.000 min^{-1}, and the resulting peaks in the signal examined. Figure 4 shows the results for the four variants of the artifacts with the cut-outs. The height of the resulting peak depends on the depth of the cut-out. The deepest cut-out

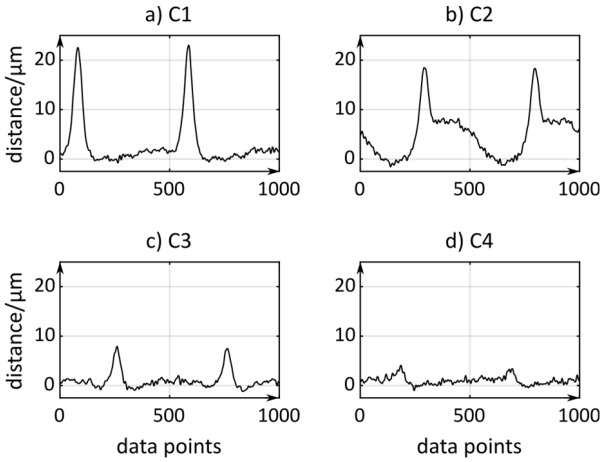

Figure 4: Sensor signals for the cut-out artifact variants.

in Figure 4 a) performs best with the highest difference between peak and average sensor value. A large difference is desirable, as this makes the peak detection more robust. With decreasing cut-out depth in Figure 4 b) and c), the peak height decreases about two- and threefold. For the lowest cut-out depth in Figure 4 d), the peak almost disappears.

The signals of the bar shaped artifacts are shown in Figure 5. As all variants performed similar, only two variants are shown. Both variants provide distinctive peaks, without any background signal. As only the material on the side of the bar is 'seen' by the sensor, the rest of the artifact is 'invisible' to it. This results in the sensor signal dropping outside its range at those locations, seen as the constant signal level in between peaks. This is an advantage over the signals of the single cut-out artifacts in Figure 4, as no background signal is present that could influence the later peak detection. The peak width is determined by the thickness of the bar, with B2 producing a broader peak, and B3 a more slender one. Both peak variants contain enough data points for peak detection.

While the length of the artifact did not have an influence on the signal, the shorter bar shaped artifacts are harder to handle. The prepared area of the artifact must be centered over the capacitive sensor very accurately, otherwise the signal peak will split into two separate peaks. Multiple iterations of positioning and measuring are needed to avoid this. With the longer bar shaped artifacts, positioning accuracy is not critical.

The artifacts with triangular shape behave very similar to the bar-shaped ones. Figure 6 a) and b) show the signals for variants T1 and T3 of the triangular artifacts, respectively. The two variants provide clearly recognizable peaks and a constant out-of-range signal in between, like the bar shaped artifacts in Figure 5. However, due to their triangular shape, these artifacts produce three peaks per revolution.

Both the bar-shaped and the triangular artifacts are preferred over the cut-out variants, since they provide sharper peaks in the sensor signal, as well as a constant out-of-range signal. The initial tests were carried out at a comparatively low 30.000 min^{-1}, and higher speeds are to be investigated in later spindle characterizations. Therefore, the exact peak form and number

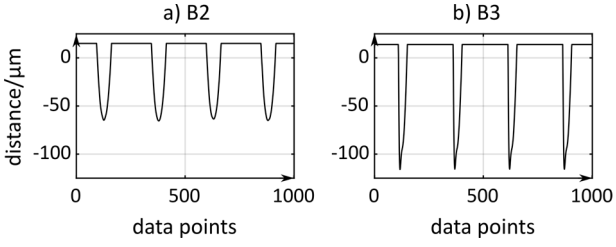

Figure 5: Sensor signals for two variants of the bar shaped artifacts.

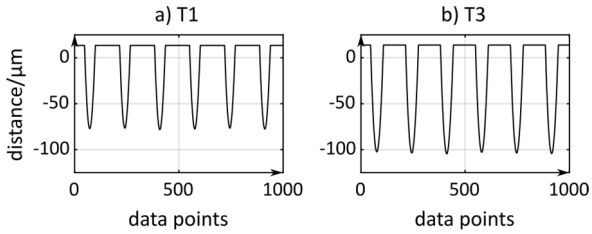

Figure 6: Sensor signals for two variants of the triangular artifacts.

of data points were examined at 100.000 min^{-1} for the two variants. Figure 7 a) and b) show a detailed view of a single peak for the bar-shaped artifact B3, and the triangular artifact T1, respectively. The bar shaped artifact in Figure 7 a) displays about half the amount of data points in the peak area versus the triangular patterned artifact in b). Even with the linear interpolation in the plots, the peak in a) is choppy, while the one in b) is almost a perfect parabola. The triangular artifacts are thus chosen for the further course of this study: The peak detection will be more precise, especially at higher spindle speeds. The wider triangular artifacts T3/T4 delivering broader, not as sharp peaks with more data points, are not required in this speed range. For spindle speeds above 200.000 min^{-1}, they can be advantageous to still provide adequate peak detection, though.

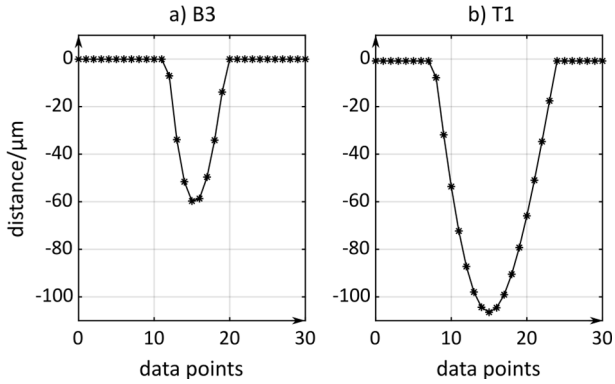

Figure 7: Captured data points at the artifact peak at 100.000 min^{-1} for the bar shaped (a)) and triangle patterned (b)) artifacts.

The triangular artifacts produce three peaks per revolution. Only every third peak must be considered as a rotational positioning mark, and the other two peaks ignored. To achieve this, the triangular pattern is combined with a cut-out at one of the triangle tips. As a result, one peak in each revolution has a significantly lower amplitude than the other two. From the amplitudes of the artifacts with the cut-out in Figure 4, a depth of 25 µm was chosen. This ensures that the peaks can be separated, but does not remove more material than necessary.

4. Angular position detection and method comparison

Figure 8 shows the resulting sensor signal using the modified triangular patterned artifact, as well as the areas defined in the peak selection in the data analysis script. A once per revolution signal is now available to reference the data points acquired from the other capacitive sensors to the spindle position. This can then be used to reliably calculate the synchronous and asynchronous error motions, as well as enable artifact separation via multisensor techniques [10; 11]. For this, the exact locations of the modified peaks of the triangular artifact need to be detected over the entire measurement signal length. The peak positions are derived from the data via a two-stage process: All three peaks are detected for the entire signal length using the minimum peak height and distance indicated in

Figure 8. The position and amplitude of the selected peaks are then saved, and the resulting vector filtered for the target peaks with lower amplitude. The result is a vector containing the indexed location of the peaks. These are then used to identify the individual revolutions for the measurement channels.

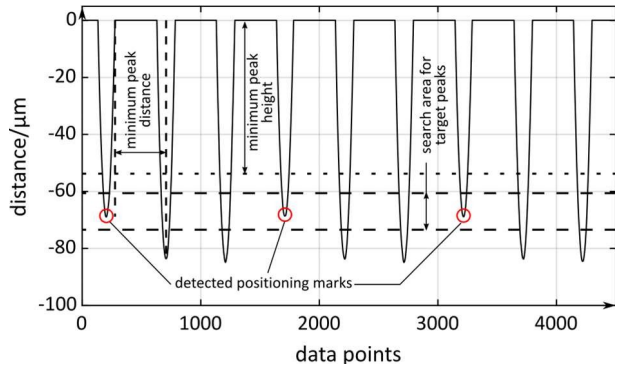

Figure 8: Peak selection via peak height of the triangle patterned artifact with cut-out.

As described in the introductory section, not all revolutions have the same amount of data points. Therefore, a linear interpolation is performed over each revolution, resampling the data to the average number of data points per revolution. This ensures a uniform data structure with constant angular spacing for all subsequent calculations. This is also crucial in eliminating the errors resulting from the overflow behavior shown in Figure 1. After these computations, the data from the sensors used to characterize the spindle is referenced correctly to the spindle's angular position. The following computations for the synchronous and asynchronous error motion for the fixed and rotating sensitive directions, as well as the total indicated runout can then be performed as usual.

The impact of the angular referencing implementation is clearly visible in Figure 9: It displays the synchronous error motion of the spindle in X-direction calculated over a large number of revolutions with and without the implementation. Without the zero-mark reference, the angular offsets between the actual and the assumed start of each revolution lead to an averaging effect: The offset increases per revolution, and the assumed angular positions 'rotate' around the actual ones. Since the synchronous error motion is the mean displacement at each angular position, the result closely resembles a circle. In contrast, the synchronous error motion with the zero-mark reference is computed correctly. While the offset between actual and assumed start of each revolution is largely eliminated, the accuracy of the method highly depends on the peak detection. Measurement noise or imperfect artefact geometry can lead to a peak being detected at a slightly different angular

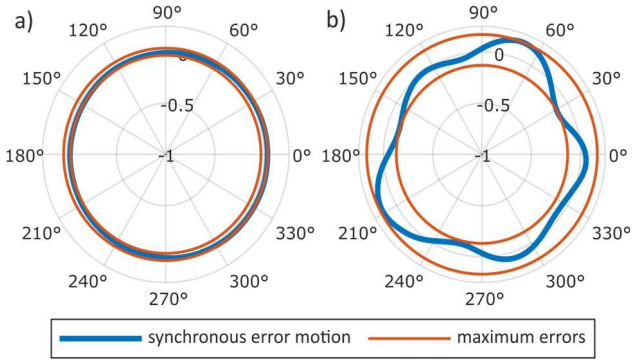

Figure 9: Comparison of the synchronous error motion in X-direction over 4000 revolutions at 100.000 min^{-1}: a) without and b) with using the zero-mark reference from the additional sensor.

position. Especially since the peaks are only defined by a few data points, this can lead to errors. In addition, the mismatch between the sampling and the spindle frequency cannot be eliminated. However, it will not accumulate over multiple revolutions using our method. As such, the precision of spindle characterizations can be enhanced, though not as much as using an encoder signal would.

5. Conclusion and outlook

In this paper, we implemented a method to reference the zero angular position of high speed spindles without rotary encoders during spindle characterizations. We used an additional displacement sensor and modified artifacts to generate a once per revolution signal, which results in a more accurate reference than the artifact out-of-roundness error. In the experiments, the triangular patterned artifacts delivered the sharpest peaks with the highest resolution. After modifying the analyzation script to utilize the additional information, we were able to reference the angular position of the spindle with good accuracy.

With the triangular artifacts, the repeatability of the method was high enough to properly reference the measured data to the angular positions of the spindle over several thousand revolutions. Therefore, we were able to eliminate the errors caused by unsynchronized data acquisition to a high degree. In further investigations we will use this method to employ error separation techniques for on-machine measurements, which heavily rely on correct angular information.

Acknowledgements

Funded by the Deutsche Forschungsgemeinschaft (DFG, German Research Foundation) - project number 407558930 - associated project SFB926 - project-ID 172116086, and project number 491400536.

[1] "Naming of specific manufacturers is done solely for the sake of completeness and does not imply an endorsement of the named companies nor that the products are necessarily the best for the purpose."

References

[1] Dornfeld D, Min S and Takeuchi Y 2006 Recent Advances in Mechanical Micromilling *CIRP Annals* **55**/2 745–68

[2] Cheng K and Huo D 2013 Micro Cutting *Wiley*

[3] Thepsonthi T. 2014 Modeling and Optimization of Micro-End Milling Process for Micro-Manufacturing

[4] Jackson M J, Robinson G M, Hyde L J, Kanjarkar K and Cui J 2007 Design and manufacture of high-speed spindles for dry micromachining applications *IJNM* **1**/5 641

[5] Anandan K P and Ozdoganlar O B 2013 Analysis of error motions of ultra-high-speed (UHS) micromachining spindles *International Journal of Machine Tools & Manufacture* **70** 1–14

[6] Bediz B, Gozen B A, Korkmaz E and Ozdoganlar O B 2014 Dynamics of ultra-high-speed (UHS) spindles used for micromachining *International Journal of Machine Tools & Manufacture* **87** 27–38

[7] Marsh E R 2010 Precision Spindle Metrology *DEStech Publications, Inc.*

[8] Bohley M, Reichenbach I G, Müller C and Aurich J C 2016 Development of a desktop machine tool for integrated ultra-small micro end mill production and application *11th International Conference on Micro Manufacturing*

[9] Aurich J C, Haberland R, Schüler G M and Engmann J 2008 Mikroschaftwerkzeuge für die Fräs- und Schleifbearbeitung *wt Werkstattstechnik online* **98**/11/12 944–9

[10] Chen Y, Zhao X, Gao W, Hu G, Zhang S and Zhang D 2017 A novel multi-probe method for separating spindle radial error from artifact roundness error *Int J Adv Manuf Technol* **93**/1-4 623–34

[11] Cappa S, Reynaerts D and Al-Bender F 2014 A sub-nanometre spindle error motion separation technique *Precision Engineering* **38**